JOURNAL OF APPLIED ELECTROCHEMISTRY **27** (1997) 317–324

Electrochemical behaviour of 1024 mild steel in slightly alkaline bicarbonate solutions

S. SIMARD, M. DROGOWSKA, H. MÉNARD

Département de Chimie, Université de Sherbrooke, Sherbrooke (Québec), Canada J1K 2R1

L. BROSSARD

Institut de recherche d'Hydro-Québec, 1800 boul. Lionel-Boulet, Varennes, Québec, Canada J3X 1S1

Received 26 January 1996; revised 29 June 1996

The electrochemical behaviour of 1024 mild steel electrodes is investigated in the presence of 0.05–0.5 M sodium bicarbonate in aqueous solution at pH 8.9 and 25 °C. Voltammograms are obtained with a rotating gold ring-mild steel electrode and the effect of the $NaHCO_3$ concentration, the potential limits and the rotation speed of the disc electrode is considered. The voltammograms display an oxidation peak current at low potentials, a passivity region and a transpassive region at high potentials for the potential sweep in the anodic direction. The oxidation current in the passivity region is practically independent of the applied potential and the $NaHCO_3$ concentration. The rate-determining step of the oxidation reaction in both the oxidation peak current region and the transpassive region is determined.

1. Introduction

In urban areas, the transformers forming part of the electric system may be operating in underground vaults. The transformer tanks are made of mild steel coated with liquid paint systems and may be in contact with residual waters (slightly alkaline) containing bicarbonate, chloride and possibly sulfate ions [1]. When the coating is damaged, the mild steel may therefore be in contact with the solution and corrosion problems are likely.

As far as bicarbonate aqueous solutions are concerned, little effort has been devoted to the study of mild steel electrodes [2, 3] compared to pure iron electrodes [4–12]. The behaviour of iron is generally investigated in slightly alkaline solutions in concentrated HCO_3^-/CO_3^{2-} aqueous solutions, whereas the characteristics of mild steel have been investigated in diluted HCO_3^-/CO_3^{2-} aqueous solutions of pH 10 or over [2, 3].

The potentiodynamic trace of stationary mild steel electrodes at pH close to 10 in the presence of 600 ppm carbonate/bicarbonate solution displays three distinct oxidation peaks. At low potentials, the first oxidation peak has been ascribed to the oxidation of iron to ferrous carbonate and hydroxide, the second to further oxidation to ferric oxide. The third anodic peak in the transpassive region has been attributed to the formation of Fe(VI) species [2, 3].

The present investigation focuses on the potentiodynamic characterization of 1024 mild steel electrodes in deaerated 0.05–0.5 M sodium bicarbonate aqueous solutions at pH 8.9 and 25 °C. The rotating gold ring-mild steel disc electrode is used to study the dissolution process for three distinct electrooxidation regions seen on voltammograms.

2. Experimental details

The experiments were carried out with a rotating disc electrode or a rotating ring-disc electrode. In both cases, the electrode was a mild steel (1024) disc whose composition is given in Table 1.

The disc electrode had a surface area of 0.126 cm^2. The rotating gold ring-steel disc electrode had a steel disc diameter of 5 mm while the gold ring had an inner diameter of 5.15 mm and an outer diameter of 7.2 mm ($N = 0.4715$ for calculated collection efficiency [13]). The disc and ring–disc electrodes were set in a Kel-F holder. The auxiliary electrode was a platinized platinum grid separated from the main compartment by a Nafion® membrane. The reference electrode was a saturated calomel electrode (SCE) connected to the cell by a bridge and a Luggin capillary. All potentials quoted below are referenced to this electrode. Since the presence of aqueous Fe(II) in the solution can eventually influence the nature of the oxide film [14], the volume of the electrochemical cell used was 0.55 L or more, so that the concentration of dissolved iron in the bulk of the solution could be neglected.

Aqueous solutions were prepared with BDHAssured® or Anachemia® analytical reactant grade chemicals using deionized water and the pH was adjusted to 8.9 by the addition of sodium hydroxide solution. The solutions were deaerated by high-purity nitrogen bubbling before and during experiments. The electrode surfaces were ground with 600, 3/0 emery paper and mechanically polished with 1.0 μm

Table 1. Weight composition (%) of 1024 mild steel

Fe	*C*	*Mn*	*P*	*S*	*Si*	*Cu*	*Ni*	*Cr*	*V*	*Mo*	*Co*	*Sn*	*Al*	*Ti*	*Nb*
98.56	0.162	0.93	0.008	0.007	0.20	0.008	0.005	0.037	0.004	0.018	0.005	0.002	0.037	0.005	0.003

and 0.05 μm alumina suspensions before each immersion.

The measurements on the rotating disc electrode were performed with a PAR 273A potentiostat controlled by computer, using M270 and M342C electrochemical softwares. The measurements with the rotating ring disc electrode were taken with a Pine Instrument Company bipotentiostat model AFRDE4 and the output signal was converted from analog to digital and recorded on an IBM-compatible computer. The rotator for the electrodes was a Pine Instrument Company analytical rotator.

3. Results

3.1. *Cyclic voltammetry*

Figure 1 shows voltammograms for a 1024 mild steel disc electrode rotated at 1000 rpm in a 0.1 M $NaHCO_3$ solution (pH 8.9). Prior each experiments, the open circuit potential was about −0.835 V and the scans were started in anodic direction from this potential. The scan rate was 0.005 Vs^{-1} and the potential limits were −0.835 and 1.5 V. At potential lower than −0.835 V, hydrogen evolution begins, and at 1.5 V, oxygen evolution is involved. The potentiodynamic traces display a large oxidation peak current at −0.65 V and a passivity region between −0.5 V and 0.9 V for the potential sweep in the anodic direction. From 0.9 to 1.5 V, a transpassive region is noticed and two waves are observed. The most anodic wave may be linked to oxygen evolution. The other wave is interpreted in the transpassive region section. The reverse sweep is characterized by a small reduction peak at about −0.75 V. The anodic current peak at −0.65 V increases with the cycle number (n) for the first three potential sweeps but decreases with n, as n becomes larger (up to 69 consecutive cycles). The height and location of the reduction peak are independent of the cycle number.

The rotating ring–disc electrode was used to detect the soluble species generated during the electrochemical oxidation of mild steel. The potential of the ring electrode was held constant at 0.4 V to oxidize the Fe^{2+} species generated at the disc electrode to Fe^{3+}. In the region of the peak oxidation current, the i/E curve for the ring electrode is similar in shape to that for the disc electrode (Fig. 2)

The charge related to the peak oxidation current noticed on the voltammogram for the steel disc electrode is approximately twice that involved in further oxidation of Fe^{2+} to Fe^{3+} at the gold ring electrode when the collection efficiency is taken into account. In the region of passivity, the current at the ring electrode is negligible compared to that at the disc electrode. The application of a constant potential of −0.9 V at the ring electrode when the mild-steel electrode is in the passivity region results in the absence of any reduction current (at the ring electrode). The absence of any soluble species generated in the passivity region is deduced.

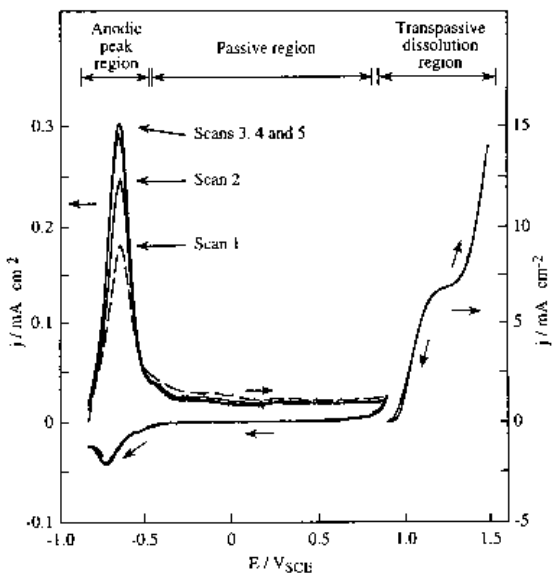

Fig. 1. Cyclic voltammograms for a 1024 mild steel electrode rotated at 1000 rpm in 0.1 M $NaHCO_3$ at pH 8.9. $dE/dt = 0.005$ V s^{-1}.

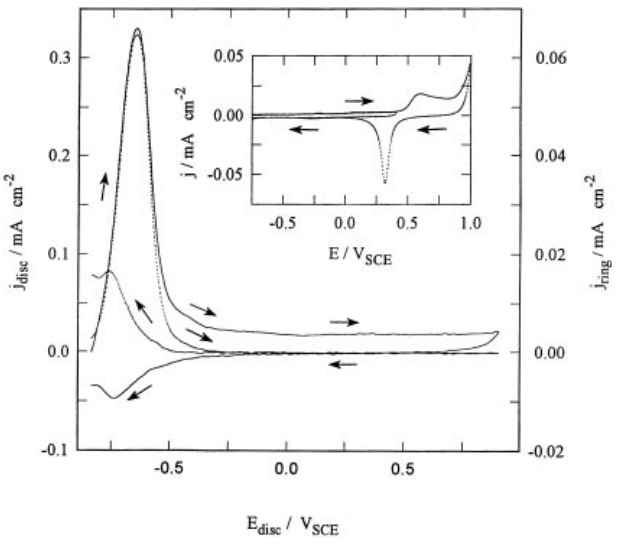

Fig. 2. Current at gold ring electrodes during potential sweep of the mild steel disc electrode. Electrode rotation speed: 1000 rpm. Solution: 0.1 M $NaHCO_3$ (pH 8.9). Disc scan rate: $dE/dt = 0.005$ V s^{-1} and $E_{Ring} = 0.4$ V. Inset: Potentiodynamic traces for gold electrode under the same experimental conditions. Scans are started at −0.75 V and anodic potential limits are 0.4 and 1 V Key: (—)J_{Disc}; (.....)J_{Ring}.

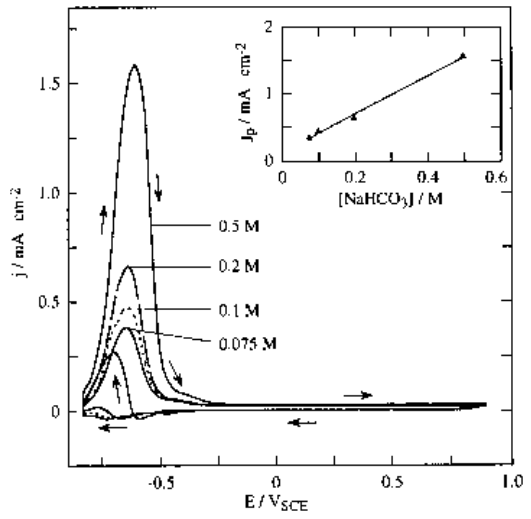

Fig. 3. Effect of bicarbonate concentration on the anodic peak at −0.65 V, $\omega = 1000$ rpm, pH = 8.9 and $dE/dt = 0.005$ V s^{-1}.

The effect of the bicarbonate concentration in the range of 0.075 to 0.5 M on the potentiodynamic behaviour of mild steel was investigated (Fig. 3). A linear relationship of the maximum peak current for stabilized potentiodynamic traces against the bicarbonate concentration was observed with J_p close to 0 for $[NaHCO_3]$ close to zero. Furthermore, the anodic current in the passive region is slightly dependent on the HCO_3^-/CO_3^{2-} concentration, which means that the stability of the oxide film is practically independent of the concentration. The broad cathodic peak noticed for the potentiodynamic traces in the cathodic direction under the experimental conditions of Fig. 1 is related to the detection of Fe^{2+} soluble species taking the form of an anodic current on the gold ring electrode (held at 0.4 V). The anodic charge noticed at the ring electrode is larger than the cathodic charge for the mild steel electrode.

i/*E* curves were also recorded for a pure iron electrode under the experimental conditions of Fig. 1. The shape of the curve and the location of the oxidation and reduction peaks are in agreement with Fig. 1. The behaviour of mild steel in a $KHCO_3/K_2CO_3$ (pH 9.5) solution is consistent with the features reported in the literature [1].

Further efforts were devoted to clarify the electrode process for the elctrooxidation of mild steel in the region of the anodic peak current (region I, from −0.835 to −0.5 V) and passivation (from −0.5 to 0.9 V).

3.2. *Anodic peak current region*

The effect of the reduction potential applied just prior to the potential sweep in the anodic direction ($E_{l.c.}$) and the polarization time (t_r) at E_r was investigated. In the region of the first anodic peak current, for E_r slightly higher than −0.84 V, the shape and height of the anodic peak current were practically independent of E_r and t_r. The picture is very different for $E_r \leq -0.84$ V. For $E_r = -0.84$ V, it is observed that the height of the oxidation peak (mild steel disc electrode) increases from $t_r = 1$ min to $t_r = 10$ min (Fig. 4), while the height of the current peak detected at the ring electrode (corresponding to the detection of soluble $Fe^{(2+)}$ species) is practically independent of t_r. This behaviour is most likely related to the adsorption and/or absorption of hydrogen on the disc surface when held at $E_r \leq -0.84$ V. Consequently, E_r was held constant at −0.835 V prior to the potential sweep in the anodic direction to minimize the influence of hydrogen generation on the oxidation processes.

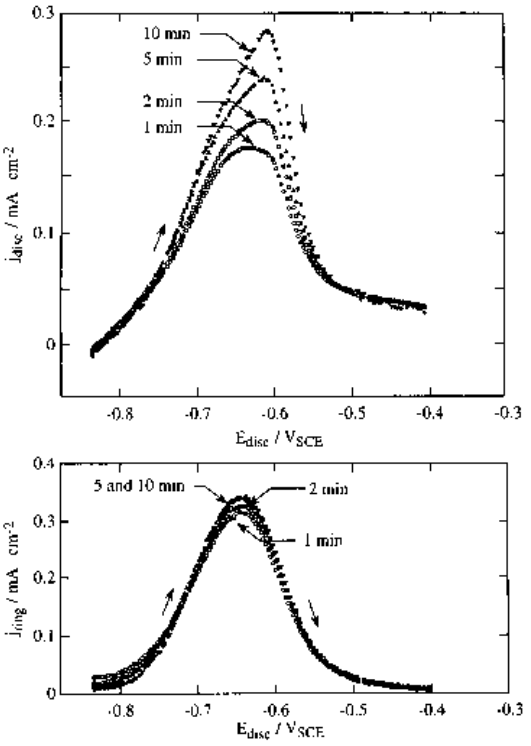

Fig. 4. Effect of polarization time at $E_r = -0.84$ V on the *i*/*E* curves for a 1024 mild steel disc-gold ring electrode rotated at 1000 rpm. $dE/dt_{(disc)} = 0.005$ V s^{-1}, 0.05 M $NaHCO_3$ (pH 8.9). $E_{Ring} = 0.4$ V.

The potentiodynamic curves of Fig. 5 for a mild steel disc electrode, with potential limits of −0.835 and −0.4 V and a sweep rate of 0.005 V s^{-1}, show

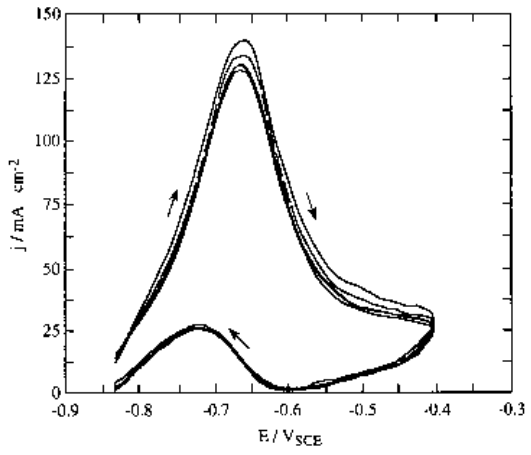

Fig. 5. Potentiodynamic traces for 1024 mild steel disc electrode rotated in 0.1 M $NaHCO_3$ (pH 8.9) at 1000 rpm. dE/dt = 0.005 V s^{-1} and potential limits of −0.835 and −0.4 V.

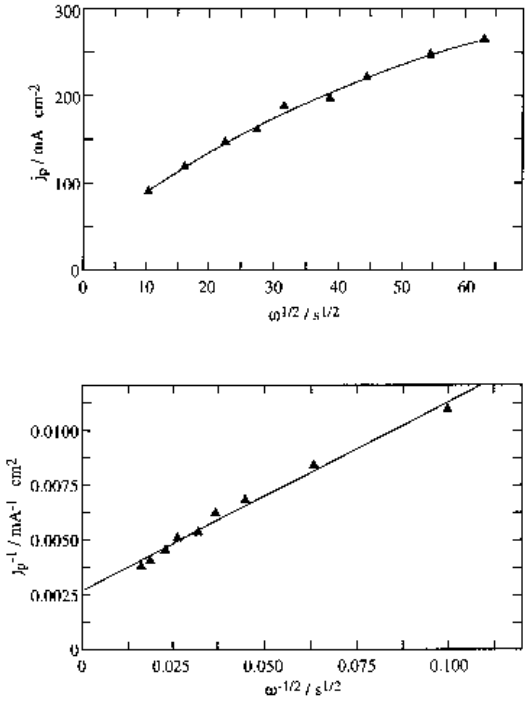

Fig. 6. j_p against $\omega^{1/2}$ and $1/j_p$ against $\omega^{-1/2}$ for a 1024 mild steel disc. Except for ω, experimental conditions are those of Fig. 5.

that cycling has practically no effect on the shape or height of the first oxidation peak; the current remains anodic during the sweep in the negative direction. Furthermore, the anodic peak current maximum (i_p) increases at higher rotation speeds of the electrode (ω) (Fig. 6).

3.3. *Passive region*

Voltammograms with the increasing positive potential limit ($E_{l.a.}$) above −0.4 V for a 1024 mild steel electrode rotated at 1000 rpm and with dE/dt of 0.005 V s^{-1} in 0.1M $NaHCO_3$ are presented in Fig. 7. For

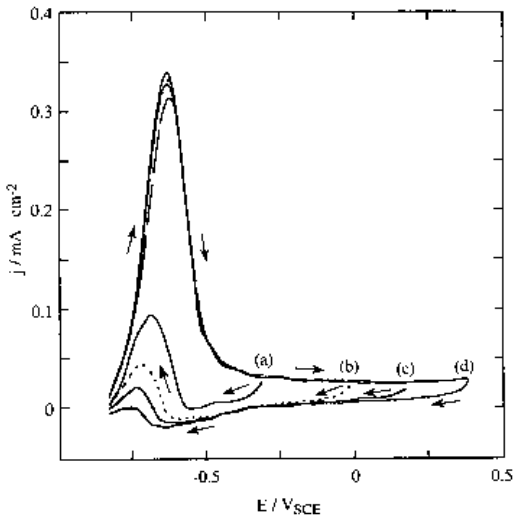

Fig. 7. Potentiodynamic curves for different positive potential limits: (a) −0.3 V, (b) 0.0 V, (c) 0.2 V and (d) 0.4 V. $\omega = 1000$ rpm. dE/dt = 0.005 V s^{-1}. Solution: 0.1 M $NaHCO_3$ (pH = 8.9).

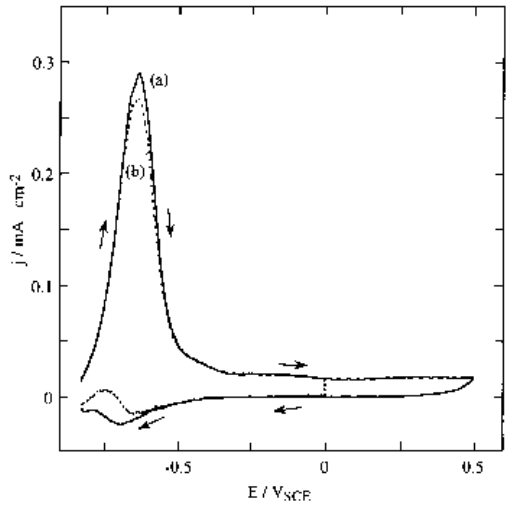

Fig. 8. Cyclic voltammogram for $E_{l.a.}$ = (a) 0.5 V and (b) 0.0 V for a 1024 mild steel electrode rotated at 1000 rpm and dE/dt = 0.005 V s^{-1} in 0.1 M $NaHCO_3$ at pH 8.9 with same anodic charge but different anodic limits.

$E_{l.a.}$= −0.3 V, an anodic peak is observed during the sweep in the negative direction with no cathodic current prior to the anodic peak. For −0.3 V < $E_{l.a.}$ <0.35 V, a broad cathodic peak current is noticed before the anodic peak current, the charge of the anodic current peak decreases, while the charge of the cathodic current peak increases as the value of $E_{l.a.}$ is raised. When $E_{l.a.}$ >0.35 V, only a cathodic current peak is observed.

In another set of experiments (Fig. 8), the electrode was polarized at a scan rate of 0.005 V s^{-1} up to 0.5 V for cycle (a) and up to 0 V for cycle (b). For cycle (b), the potential of 0 V was maintained until the accumulation of 1.3 mC cm^{-2} to obtain the same charge as for cycle (a). The potentiodynamic traces for the potential sweep in the cathodic direction are slightly different for the two cycles, with a lower cathodic charge and a smaller anodic peak current for cycle (b).

3.4. *Transpassive region*

The electrochemical behaviour of mild steel was characterized in the transpassive region for 0.1 M $NaHCO_3$ solution at pH 8.9. In one set of experiments, the disc electrode potential was swept from 0.9 to 1.5 V at 0.005 V s^{-1} and the gold ring electrode potential was held at −1.035 V to measure the current linked to the reduction of soluble iron species. It is relevant to point out that the hydrogen evolution reaction on a gold ring electrode is negligible for E_r = –1.035 V. The higher the anodic current at the disc electrode, the higher the reduction current at the ring electrode, which indicates that soluble iron species are generated in the transpassive region (Fig. 9).

At any given potential value, the anodic current observed on the disk electrode in the transpassive region was dependent on the rotation frequency with a linear relationship of j_l against $\omega^{1/2}$ and $j_l \to 0$ for $\omega \to 0$ (Fig. 10).

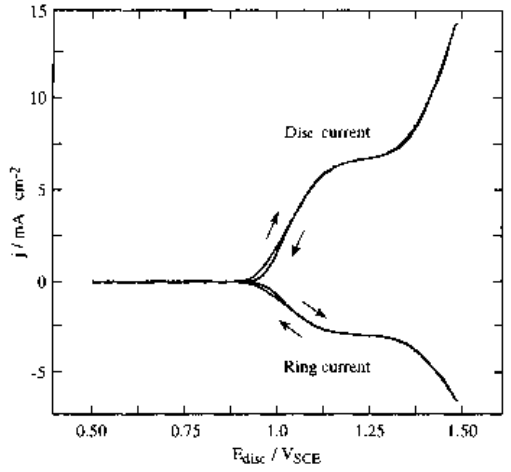

Fig. 9. Cyclic voltammogram for 1024 mild steel disc electrode in the transpassive region and the response at the gold ring electrode. $\omega = 1000$ rpm. $dE/dt_{(disc)} = 0.005$ V s^{-1}. $E_{ring} = -1.035$ V. Solution: 0.1 M $NaHCO_3$ (pH = 8.9).

In a second set of experiments, the potential of the 1024 mild steel disc electrode was held constant at 1.2 V while the potential of the gold ring electrode was swept at 0.005 V s^{-1} from 0.4 V to –1.035 V. On the ring electrode, two reduction current waves were observed with half-wave potentials at about −0.25 V for wave I and about −0.7 V for wave II (Fig. 11). At the end of the potential sweep, at –1.035 V, an electrodeposit of iron was noticed on the gold ring electrode. The reduction waves observed in this set of experiments may possibly be related to the following reaction: Fe (III) + e^- → Fe (II) for wave I and Fe (II) + $2e^-$ → Fe(0) for wave II. The absence of a reduction wave related to the presence of a ferrate species is most likely linked to their rapid decomposition. To evidence the presence of ferrate species during mild steel preanodization, a potential of 1.2 V was applied to a stationary electrode for 2 s, just prior to the potential sweep in the cathodic direction at a scan rate of 20 V s^{-1} and a starting potential of 0.95 V. The potentiodynamic curves are illustrated in Fig. 12 for the preanodization (2 s) and without preanodization (0 s). A broad reduction peak current located at 0.75 V is observed for a 2 s preanodization time, which is ascribed to the reduction of ferrates generated during preanodization. On the other hand,

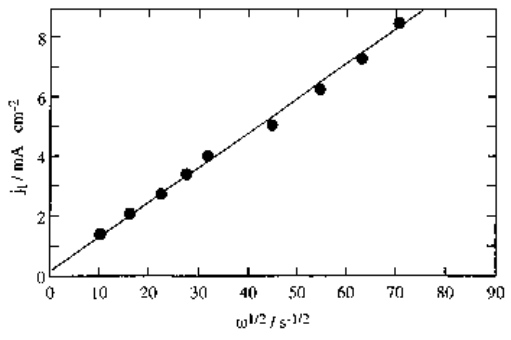

Fig. 10. Limit current density of ferrate dissolution wave (j_l) as a function of frequency ($\omega^{1/2}$) for 1024 mild steel electrode rotated at 1000 rpm in 0.1 M $NaHCO_3$ and pH 8.9 at $E_{disc} = 1.2$ V.

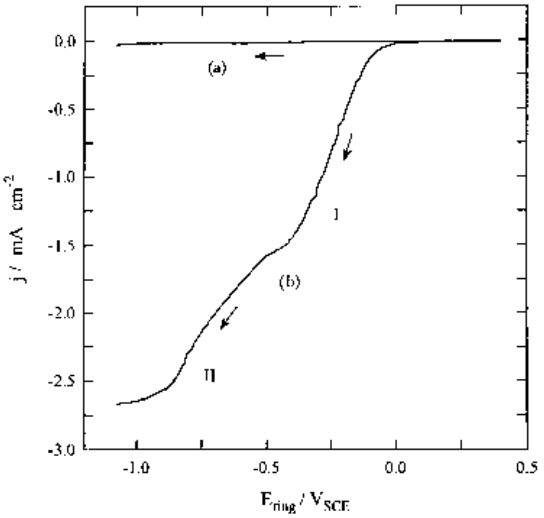

Fig. 11. Linear voltammogram for gold ring electrode. $\omega = 1000$ rpm. Solution: 0.1 M $NaHCO_3$ (pH 8.9) and ring scan rate of $dE/dt_{(ring)} = 0.005$ V s^{-1}. (a) E_{Disc} = Open-circuit potential. (b) E_{disc} = 1.2 V.

no reduction current is observed for 0 s preanodization time.

3.5. *Transient behaviour after potentiostatic preanodization*

The protective film formed during preanodization of a 1024 mild steel rotating disc electrode at 0.8 V in 0.05 to 0.5 M $NaHCO_3$ solutions (pH 8.9) was further characterized by recording the transient potential against time under open-circuit and galvanostatic conditions. Preanodization lasted about 3 h in such a way that the (anodic) charge involved during preanodization reached about 10 mC cm^{-2} before interruption. Immediately afterwards, transient potential against time were recorded under open-circuit and galvanostatic conditions.

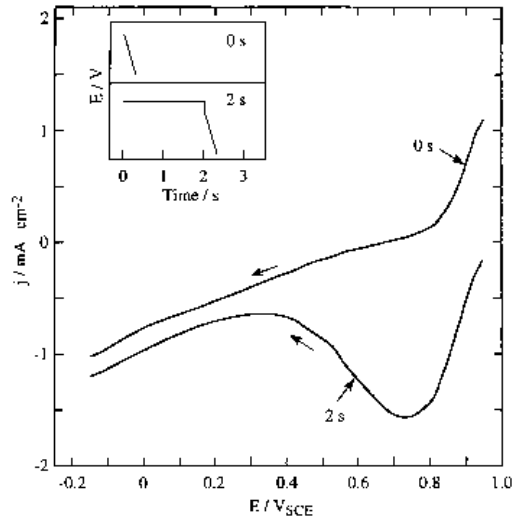

Fig. 12. Potentiodynamic trace for the cathodic potential sweep at 20 V s^{-1} with and without preanodization at 1.2 V for 1024 mild steel disc electrode. $\omega = 1000$ rpm. Solution: 0.1 M $NaHCO_3$ (pH = 8.9). $dE/dt = 20$ Vs^{-1}.

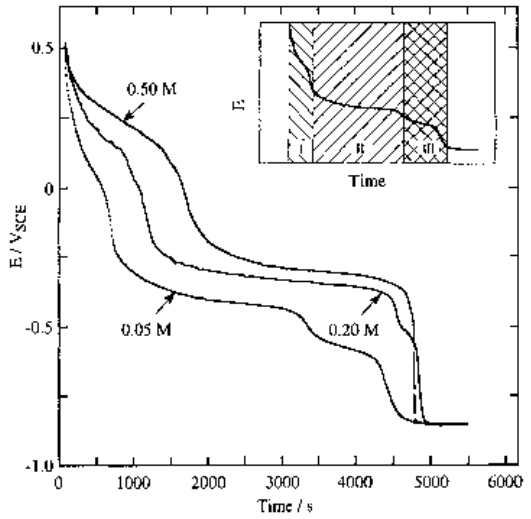

Fig. 13. Open-circuit potential transients after preanodization of 1024 mild disc electrode. $\omega = 1000$ rpm. pH 8.9. Preanodization at 0.8 V for 3 h ($Q \sim 10$ mC cm^{-2}).

Under open-circuit potential conditions, potential transients were recorded for three different $NaHCO_3$ concentrations (Fig. 13). For 0.5 M $NaHCO_3$, two potential steps (~ 0.2 and ~ −0.3 V) are observed. The shape of the potential against time curves is approximately the same, regardless of the $NaHCO_3$ concentration, and the lower the $NaHCO_3$ concentration, the higher the rate of potential decrease. For the three $NaHCO_3$ concentrations, a constant negative potential of −0.85 V was attained after approximately 5000 s. In the galvanostatic measurements, two plateaus are distinguishable under a weak cathodic current of 800 nA cm^{-2} (Fig. 14). The total reduction charges to reach the potential of the bare metal is 200 μC cm^{-2} for 0.1 M $NaHCO_3$, 160 μC cm^{-2} for 0.2 M $NaHCO_3$ and 135 μC cm^{-2} for 0.5 M $NaHCO_3$, that is, the reduction charge is negligible compared to the oxidation charge prior to reduction.

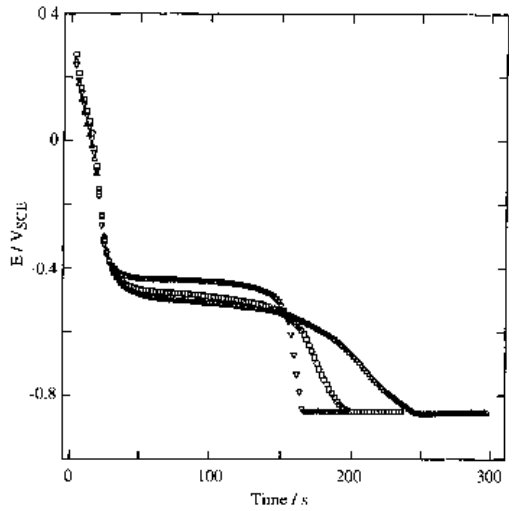

Fig. 14. Chronopotentiometric curves recorded under a reduction current of 800 nA cm^{-2} after preanodization. 1024 mild steel disc electrode. $\omega = 1000$ rpm. pH 8.9. Preanodization at 0.8 V for 3 h ($Q \sim 10$ mC cm^{-2}). Key: (∇) 0.5 M $NaHCO_3$; ($\square$) 0.20 M $NaHCO_3$; ($\triangle$) 0.10 M $NaHCO_3$.

The rate of potential decrease is higher with the small applied reduction current compared to the open-circuit potential curves.

In open-circuit potential transients, it is observed that more time is required to remove the solid species in step I as the concentration of $NaHCO_3$ increases (Fig. 13). On the other hand, Fig. 14 shows that the corresponding galvanostatic step I for all curves has the same charge; the amount of the species in the film linked to step I is consequently independent of the bicarbonate concentration.

Under open-circuit conditions, the length of the potential transients associated with step II was independent of the bicarbonate concentration. For step III, in the galvanostatic (where the transient appears as a change of the negative slope at the end of step II) and in open-circuit potential measurements, the reduction time decreases with an increase in the bicarbonate solution concentration. The potential of −0.85 V takes about 20 times longer to reach in the open-circuit measurements than in the galvanostatic measurements. This implies that the amount of oxide in these films is small.

4. Discussion

The following features are deduced from the potentiodynamic characteristics observed at the disc and disc-ring electrodes:

(i) The high anodic dissolution peak current at −0.65 V on the potentiodynamic traces (Fig.1) is related to the electrodissolution of iron (Fig. 2), most likely in the form of soluble $FeHCO_3^+$ (aq) and /or Fe(II) (aq) [4] with no significant amount of oxides accumulated on the surface.

(ii) It is deduced that HCO_3^-/CO_3^{2-} species participate in the oxidation reaction, since the relationship of j_p against [$NaHCO_3$] (Fig. 3) is linear in the region of the first oxidation peak. This is consistent with the formation of Fe^{2+} —HCO_3^-/CO_3^{2-} complexes, most likely $FeHCO_3^+$ (aq). The linear relationship of i_p^{-1} against $\omega^{-1/2}$ with $i_p^{-1} \neq 0$ at $\omega^{-1/2} \rightarrow 0$ (Fig. 6) suggests that the diffusion of ionic species at the electrode surface plays a key role in limiting the oxidation process.

The dissolution process of the mild steel electrode is due to the formation of soluble species with iron at a valency of +2, that is, $FeHCO_3^+$ (aq) and/or Fe(II) (aq). By contrast, for work on pure iron, the recovery of the dissolved iron species is approximately half the theoretical value when the collection coefficient is taken into account [4]. This implies the formation of insoluble iron species; for example, $FeCO_3$(s), during the active dissolution of pure iron. The higher pH and solution concentration used to investigate the behaviour of pure iron electrodes promote the formation of insoluble iron species in the active-dissolution region and may explain the behaviour observed for pure iron and mild steel electrodes.

The formation of iron complexes is possible through the following overall reaction:

$$Fe(0)(s) + HCO_3^-(aq) \Leftrightarrow FeHCO_3^+(aq) + 2e^- \quad (1)$$

with an equilibrium between dissolved species [4]:

$$FeHCO_3^+(aq) \Leftrightarrow Fe(II)(aq) + HCO_3^-(aq) \quad (2)$$

the precipitation of $FeCO_3(s)$ being promoted when the pH and concentration in CO_3^{2-}/HCO_3^- are high enough:

$$Fe(II)(aq) + CO_3^{2-}(aq) \Leftrightarrow FeCO_3(s) \quad (3)$$

The formation of $FeCO_3$ is predicted by Pourbaix diagram [15]. Spectroscopic data supporting its formation have been reported in previous works [4, 9]. Reaction 3 is marginal in the present study because $FeCO_3$ formation is induced by local high concentration of bicarbonate-iron complexes leading to precipitation. In the present investigation, the use of rotating electrode avoid any significant increasing of concentration of soluble species at the vicinity of the electrode and avoid such precipitation process.

Passivation of the mild steel electrode as the potential becomes sufficiently anodic is ascribed to the formation of a γ-Fe_2O_3 /Fe_3O_4 film [16]. This film is not affected by the presence of HCO_3^-/CO_3^{2-} as long as the applied potential remains in the passivity region, since the oxidation current is practically independent of the HCO_3^-/CO_3^{2-} concentration (Fig. 3). However, the characteristics of the potentiodynamic trace for the potential sweep in the cathodic direction after passivation are dependent of the reversal potential (Fig. 7); for low $E_{l.a.}$ values, an anodic current peak is noticed on the potentiodynamic scan in the cathodic direction, which indicates that changes are occurring in the passive film as $E_{l.a.}$ becomes more anodic. Moreover, when a cathodic wave alone is present on the mild steel electrode, a large current is detected at the ring electrode (Fig. 2), indicating the dissolution of iron during the reduction of the passive film. At the beginning of the cathodic wave located at about −0.75 V, the symmetry between the disc and the ring trace indicates that the oxide film is composed of oxides with an oxidation state higher than +2 for iron, which is consistent with the literature [16]. It is also observed that the ring current reaches a value higher than that expected when the single source of Fe(II)(aq) considered is reduction of the passive film. It is deduced that iron dissolution observed during reduction of the film is induced by the passive- film reduction combined with its breakdown, allowing oxidation (dissolution) of the bare metal (Fe→Fe(II)(aq)).

The electrooxidation current observed in the transpassive region is entirely ascribed to iron dissolution by ferrate ion formation (Fig. 12) [2, 3]. The rate-determining step of the process is the diffusion of dissolved species into the solution at the electrode surface, since the i_l against $\omega^{1/2}$ relationship with $i_l \to 0$ for $\omega^{1/2} \to 0$ is linear (Fig. 10).

An anodic current peak on the mild steel electrode in the transpassive region was reported and discussed by Rangel *et al*. [2, 3]. The peak is located at 1.1 V in NaOH and carbonate/bicarbonate solutions at pH ranging from 10 to 13. The peak increases at higher solution pH but, in the presence of carbonate/bicarbonate ions, the anodic current is even higher at lower pH than in the NaOH solution; this phenomenon is linked to the formation of ferrate species from the transpassive dissolution of the oxide film. In the present study, at pH 8.9 and different solution concentrations, an anodic current wave is observed rather than a peak. The formation of soluble Fe(III) species at the disc electrode is deduced from measurements at the gold ring electrode.

Species generated at the disc are reducible in two steps (Fig. 11). The second wave observed should be attributed to the reduction of $Fe^{(2+)}$ species to $Fe^{(0)}$, which is consistent with the electroplated iron found on the ring surface after reduction at –1.035 V during a sufficient time; it is linked to the shape of the voltammogram on the gold ring electrode after few minutes of deposition at cathodic potential while the disc potential is fixed at 1.2 V. Its shape is the same than the one for the pure iron. Hence, it can be deduced that the first wave, located around −0.25 V, is due to the reduction of $Fe^{(3+)}$ to $Fe^{(2+)}$ species. This means that no ferrates are detected directly at the ring electrode, which is explained by the instability of ferrates which decompose when water is present [17] or may be stable in solution with pH around 14 [18]. In the present work, the pH is much lower (8.9) and the stabilization of ferrates is not promoted. However, the presence of ferrates is confirmed by voltammetry at fast sweep rates (Fig. 12).

From galvanostatic and open-circuit measurements, it is deduced that the anodic film produced by preanodization at 0.8 V is a mixture of different oxides (Figs 13 and 14). The first step, observed by both techniques, is most likely linked to the reduction of γ-Fe_2O_3 [19, 21]. The second step can be linked to the formation of a lower-valency oxide corresponding to Fe_3O_4 [15, 19] and the third step to the reduction of $Fe(OH)_2$ or $FeCO_3$ [15].

The behaviour of the film in open-circuit and galvanostatic measurements suggests a sandwich-type film [19, 20]. However, reduction of this film gives a charge close to 150 μC cm^{-2}, which charge corresponds approximately to the formation of one monolayer oxide film. Consequently, it is deduced that the formation of a sandwich-type film is questionable.

5. Conclusion

The potentiodynamic curves of a 1024 mild steel electrode in aqueous solution of pH 8.9 containing dissolved sodium bicarbonate display an oxidation peak region at low potentials, a passivity region and a transpassive region at high potentials for the potential sweep in the anodic direction. The diffusion of

ionic species into the solution in the vicinity of the electrode surface plays a key role in limiting the electrodissolution process in the oxidation peak and transpassive dissolution region. It is postulated that the ionic species involved in the diffusion process is most likely $FeHCO_3^+$ (aq) in the oxidation peak region and ferrate ions in the transpassive region. The passive film obtained is thin and its nature is linked to the applied potential.

Acknowledgements

The authors acknowledge the financial support of Hydro-Québec (IREQ), Natural Sciences and Engineering Research Council of Canada (NSERCC) and Fonds pour la Formation de Chercheurs et l'Aide à la Recherche (FCAR-Québec).

References

[1] R. Gilbert, Institut de recherche d'Hydro-Québec, Internal Report IREQ-4150B (1988); G. Larochelle, L. Brossard and P. Courchesne. Internal Report IREQ-4529 (1989).
[2] C. M. Rangel, R. A. Leitao and I. T. Fonseca, *Electrochim. Acta*, **34** (1989) 255.
[3] *Idem*, *ibid.* **31**, (1986) 1659.
[4] E. B. Castro, J. R. Vilche and A. J. Arvia, *Corros. Sci.* **32** (1991) 37.
[5] E. B. Castro, C. R. Valentini, C. A. Moina, J. R. Vilche and A. J. Arvia, *ibid.* **26** (1986) 781.
[6] P. Southworth, A. Hamnett, A. M. Riley and J. M. Sykes, *ibid.* **28** (1988) 1139.
[7] J. G. N. Thomas, T. J. Nurse and R. Walker, *Br. Corros. J.* **5** (1970) 87.
[8] C. R. Valentini, C. A. Moina, J. R. Vilche and A. J. Arvia *Corros. Sci.* **25** (1985) 985.
[9] J. Gui and T. M. Devine, *ibid.* **37** (1995) 1177.
[10] D. H. Davies and G. T. Burstein, *Corrosion* **36** (1980) 417.
[11] R. D. Armstrong and A. C. Coates, *Electroanal. Chem. and Interf. Electrochem.* **50** (1974) 303.
[12] J. M. Blengino, M. Keddam, J. P. Labbe and L. Robbiola, *Corros. Sci.* **37** (1995) 621.
[13] W. J. Albery and M. L. Hitchman, 'Ring-disc Electrodes' Clarendon Press, Oxford (1971).
[14] M. E. Brett, K. M. Parkin and M. J. Graham, *J. Electrochem. Soc.* (1986) 2032.
[15] E. Deltombe and M. Pourbaix, *in* 'Comportement électrochimique du fer en solution carbonique, diagrammes d'équilibre tension-pH du système Fe-CO_2-H_2O, à 25 °C'. Rapport technique 8. CEBELCOR (1954).
[16] B. R. MacDougall and M. J. Graham, in 'Corrosion Mechanisms in Theory and Practice' (edited by P. Marcus and J. Oudar), Marcel Dekker, New York (1995).
[17] M. L. Hoppe, E. O. Schlemper and R. K. Murmann, *Acta Cryst*. **B38** (1982) 2237.
[18] K. Bouzek and I. Rousar, *Electrochim. Acta* **38** (1993) 1717.
[19] M. Nagayama and M. Cohen, J. *Electrochem. Soc*. (1962) 781.
[20] *Idem, ibid.* (1963) 670.
[21] J. A. Bardwell, B. R. MacDougall and M. J. Graham, *ibid.* (1988) 413.